ACS Catalysis

Research Article

pubs.acs.org/acscatalysis

Water–Gas Shift Catalysis at Corner Atoms of Pt Clusters in Contact with a TiO_2 (110) Support Surface

Salai Cheettu Ammal and Andreas Heyden*

Department of Chemical Engineering, University of South Carolina, 301 South Main Street, Columbia, South Carolina 29208, United States

Supporting Information

ABSTRACT: The redox and associative carboxyl pathways of the water–gas shift reaction have been investigated at a corner Pt site of the Pt/TiO_2 (110) interface using density functional theory and microkinetic modeling techniques. Overall rates calculated from the microkinetic model suggest that the redox pathway dominates in the temperature range of 473–673 K and that the oxygen vacancy structure plays a critical role in dissociating H_2O. Because of the strong adsorption of CO at the corner Pt atoms, these sites are less active than the edge Pt sites at low temperatures; however, the activity of corner atoms becomes higher above 573 K. The CO adsorption strength and the ability to dissociate H_2O are the two main factors that determine the activity of a particular site or catalyst for the water–gas shift reaction.

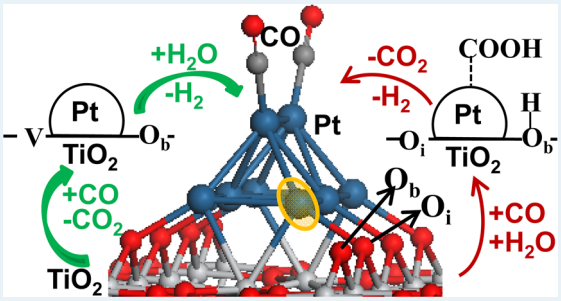

KEYWORDS: *water–gas shift reaction, microkinetic modeling, interface catalysis, corner Pt atoms, DFT*

1. INTRODUCTION

Precious metal nanoparticles supported on high surface area oxides have been shown to be highly effective and selective for many important catalytic reactions. The nanosize of the metal particles ensures that most of the expensive metal is available at the surface for catalysis. The role of the oxide support has long been thought to simply provide a platform to prevent the nanoparticles from washing away during reaction and to inhibit particle growth or sintering. In a few cases, it was suggested that the support might alter the catalytic properties by changing the shape or electronic structure of the metal. Only for a minority of catalytic systems was the metal–oxide interface region invoked as the active site for catalysis.[1] Although the importance of metal–oxide interfaces has long been recognized,[2,3] the molecular determination of their role and properties is only now emerging.[4−6] Different kinds of metal atoms, ranging from metallic to ionic, are available at the interface. These metal atoms together with the boundary oxide sites create unique reaction sites at the interface that can promote a bifunctional reaction mechanism. In our recent work, we have shown the importance of these metal–oxide interface sites for the water–gas shift (WGS) reaction ($CO + H_2O \rightleftharpoons CO_2 + H_2$) over Pt/TiO_2 (110) and Pt/CeO_2 (111) catalysts using a combination of density functional theory and microkinetic modeling techniques.[7−9]

The WGS reaction is widely used in industrial hydrogen production as well as in fuel processing for fuel cell applications.[10,11] Although the current industrial Cu-based low-temperature shift (LTS) catalysts work well for stationary applications, there is a continuous search for new and more efficient WGS catalysts for mobile fuel cell applications because of the complexities involved in the start-up/shut-down cycles as well as the pyrophoric nature of Cu-based catalysts. Supported Au and Pt catalysts have attracted much attention over the past decade because of their high activity and selectivity at low and medium temperatures. On reducible oxide supports, such as TiO_2 and CeO_2, these catalysts are expected to be bifunctional in that the noble metal adsorbs and/or activates CO and the oxide support activates H_2O.[12−15] The direct involvement of the metal–oxide interface sites in the WGS reaction mechanism has been suggested on the basis of the fact that at least for Au, the reaction rate scales linearly with the low-coordination Au atoms at the interface.[16,17] Also, nearly metal-free Au and Pt on ceria catalysts[18,19] and inversely supported catalysts of TiO_x and CeO_x nanoparticles grown on a Au(111) substrate[20,21] display significant catalytic activity for the WGS reaction. Although these studies suggest the importance of metal–oxide interface sites in these catalytic systems, the dominant reaction pathway and the nature of the exact active site involved in the WGS reaction mechanism are still controversial. Ribeiro and co-workers have conducted a series of experiments on the WGS reaction catalyzed by Au and Pt supported on various oxides and suggested that the metal atoms remain in a metallic state during catalysis and that only the metallic corner atoms are the active sites in the Au clusters.[16,17,22−24] With regard to the mechanism of the WGS reaction, two main reaction pathways, the redox[22,25−28] and associative pathways,[29,30] have been proposed at the metal–oxide interface. In the redox pathway

Received: July 8, 2014
Revised: September 4, 2014
Published: September 8, 2014

   dx.doi.org/10.1021/cs5009706 | ACS Catal. 2014, 4, 3654–3662

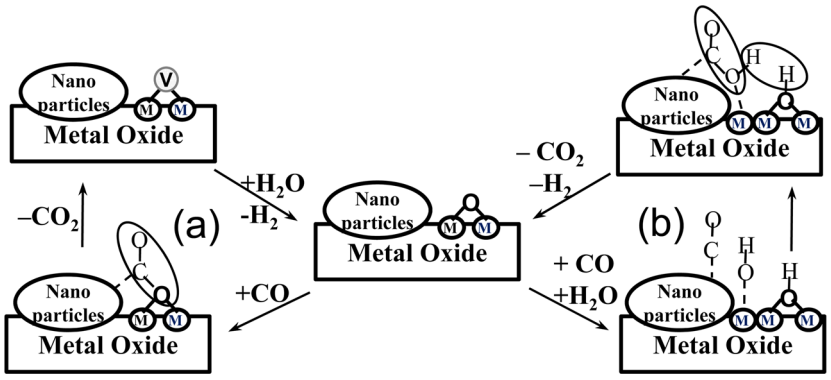

Figure 1. Proposed reaction pathways for the WGS reaction at the metal–oxide interface: (a) redox pathway and (b) associative pathway.

(Figure 1a), CO reacts with the support oxygen forming CO_2 and an oxygen vacancy in the support (Mars-van Krevelen mechanism). The reduced support is then oxidized by H_2O, forming H_2. During the associative process (Figure 1b), the formation of a carboxyl/formate intermediate must precede the production of H_2 and CO_2 and the support oxygen is not removed during the catalytic cycle. A combination of these two pathways, known as the associative pathway with redox regeneration (or equivalently, OH group regeneration), has also been suggested in the literature.[25,31−34]

Our recent work on the WGS reaction mechanism at the Pt/CeO_2 (111) interface suggested that both the redox pathway and associative pathway with redox regeneration could operate on Pt/CeO_2 catalysts.[8] In contrast, the associative pathway that does not involve the creation of an oxygen vacancy during the catalytic cycle has an activation barrier higher than that of and a rate lower than that of the redox pathways.[9] This suggested that interface oxygen vacancies are highly important in the WGS reaction mechanism for promoting H_2O dissociation as well as stabilizing key intermediates such as adsorbed -COOH and its adsorbed dissociated product, -CO_2. The Pt_{10} cluster model used in these studies has a symmetric structure with equivalent interface Pt atoms, and thus, the same active site is used to investigate all pathways mentioned above. On the other hand, the Pt_8 cluster model (Figure 2) we chose on the basis of our *ab initio* thermodynamic analysis[35] to investigate the WGS reaction at the Pt/TiO_2 (110) interface has two distinct active sites at the interface. This model consists of four undercoordinated corner Pt atoms and two edge Pt atoms at the interface. We recently reported the WGS activity of these edge Pt atoms by investigating the redox and -OH regeneration pathways.[7] It was not possible to investigate the associative pathways at these sites because the empty Ti site required for H_2O dissociation is located far from these edge Pt atoms. Here, we examine the activity of the corner interface Pt atoms for the WGS reaction by considering both the redox and associative pathways. Overall, we find that the undercoordinated corner atoms are less active than the edge Pt atoms at low temperatures because of strong CO adsorption at the corner atoms.

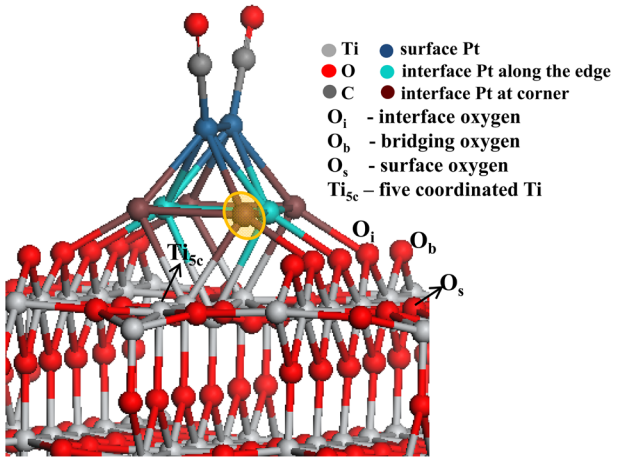

Figure 2. Pt/TiO_2 (110) catalyst model used to study the WGS reaction mechanism. The highlighted area corresponds to the initial active site.

2. COMPUTATIONAL MODEL AND METHODS

We choose in this study the same catalyst model used in our previous report[7] for the investigation of the WGS reaction mechanism at the Pt/TiO_2 (110) interface, except that the active site considered here is the corner Pt atom (Figure 2). This model was chosen on the basis of our previous constrained *ab initio* thermodynamic analysis on the stability of the Pt/TiO_2 (110) surface under WGS reaction conditions.[35] This model consists of a Pt_8 cluster covered by CO molecules on the top sites and supported on a stoichiometric TiO_2 (110) surface. Our *ab initio* thermodynamic analysis[35] of a series of Pt_n/TiO_2 (n = 1−8) clusters suggested that the oxygen vacancy formation energy at the interface converges well with cluster size for the Pt_8 cluster. In addition, experimental studies[23,33,36] identified that Pt/TiO_2 and Pt/CeO_2 catalysts containing 2−3 nm metallic Pt and 0.5−0.6 nm small Pt clusters on the oxide surface all exhibit a low-temperature WGS activity. Although conventional catalyst preparation methods usually lead to a broad distribution of comparatively large nanoparticles on support surfaces, Fu et al.[18] were able to produce well-dispersed small Pt species on high surface area ceria by leaching the catalyst samples prepared by conventional methods. Interestingly, they found the same WGS activity for both the leached and parent catalysts, which illustrates that likely only metal clusters that are also present in the leached sample were responsible for the reaction. On the basis of these experimental reports and our *ab initio* thermodynamic analysis, we believe that the results presented here for the Pt_8 cluster can also be extrapolated to larger supported nanoparticles. Smaller, two-dimensional Pt clusters will likely display a different catalytic behavior.

On the support side, experimental studies[23,28,37] have used different structures of the TiO_2 support such as rutile, anatase,

dx.doi.org/10.1021/cs5009706 | ACS Catal. 2014, 4, 3654−3662

or a mixture of anatase and rutile crystallites (Degussa P25). The WGS activity of Pt nanoparticles supported on these different TiO_2 supports was found to be very similar, as shown in the Results and Discussion (Table 2). Thus, we chose the rutile TiO_2 (110) slab model for our calculations. The TiO_2 (110) slab is modeled by a p(6 × 2) unit cell, a 17 Å vacuum gap, and 12 atomic layers with the bottom three layers fixed in their bulk positions. We used the periodic plane wave code VASP 5.2[38−41] for all calculations discussed in this work. The density functional theory (DFT) exchange-correlation term was described by the semilocal generalized gradient approximation density functional of Perdew, Burke, and Ezhernof (PBE),[42] and the core−electronic states were described by projector augmented wave (PAW) potentials.[43,44] Considering the large unit cell used in the calculations, we sampled the Brillouin zone at the Γ point only and used Gaussian smearing of the Fermi surface with a smearing width of 0.05 eV for integration of the Brillouin zone. The cutoff in the plane wave expansion was 400 eV. The numbers of valence electrons considered for Ti, O, Pt, C, and H are 10, 6, 10, 4, and 1, respectively. Dipole and quadrupole corrections to the energy are taken into account using a modified version of the method of Makov and Payne.[45] Harris-Foulke-type corrections[46] have been included for the forces. The transition state (TS) structures are optimized using the climbing image NEB[47] and Dimer methods.[48,49] We have shown in our earlier report that the differences in reaction energies calculated with the DFT + U method (U = 3 or 4 eV) and the DFT method used here for the elementary steps involving oxygen vacancy formation are less than 0.2 eV.[7] Thus, we do not expect our conclusions or trends reported in this paper to be affected by the DFT functional.

A detailed description of the microkinetic modeling approach used in this study can be found in our recent report.[7] Harmonic transition state theory and collision theory with a sticking coefficient of 1 were used to calculate rate constants for elementary surface reactions and adsorption processes, respectively. The zero-point energy (ZPE) is obtained as $\sum_i (1/2)h\upsilon_i$ from calculated vibrational frequencies, υ_i. The frequency calculations include only the gas phase molecules and a few oxygen and H atoms on the TiO_2 surface that are directly involved in the reaction mechanism. Displacements of ±0.001 Å were used along the x, y, and z directions for all Hessian constructions from analytic gradients. Considering that the harmonic approximation is least accurate for small vibrational frequencies, we shifted all (real) frequencies below 50 cm^{-1} to 50 cm^{-1}. This procedure ensures that for surface reactions low-frequency modes have no effect on reaction energies and rate constants (these frequencies in effect cancel out). After calculating the forward and reverse rate constants for each elementary reaction, we constructed a Master equation and solved for the mean field steady state solution of probability densities for the system to occupy each discrete state. We call these probability densities interface coverages, θ. The steady state equations were solved using the Maple software to obtain the interface coverages. We note here that although some of the reactant or product states in the elementary reactions are represented for the sake of clarity as having multiple species, in the Master equation each reactant or product state constitutes one discrete state. The reaction rate (turnover frequency) of each pathway was calculated using the interface coverages. The rate-controling steps and the most important reaction intermediates were identified using Campbell's degree of rate control and degree of thermodynamic rate control analyses.[50]

3. RESULTS AND DISCUSSION

3.1. Associative Pathway. Experimental studies based on FTIR and DRIFTS measurements have suggested that associative pathways with formate, carboxyl, and carbonate intermediates are likely important for the WGS reaction.[11,29,30,51−56] Supported Au catalysts,[11,29,30] Pt steps[57] and terraces,[58] and Pt supported on CeO_2[25,54−56] are a few examples for which experimental and computational studies provided evidence of the associative mechanism of the WGS reaction. However, in a recent analysis, Burch and co-workers[59] concluded that formates observed by IR were potentially the main reaction intermediates only in the case of catalysts with very low activity. For catalysts with high activity, the formates seen by IR spectroscopy typically account for less than approximately 10−15% of the total WGS reaction products. In agreement with this analysis, our mechanistic investigation of the WGS reaction at Pt/CeO_2 (111) interface sites also predicted a lower but non-negligible rate for the associative carboxyl pathway compared to that of the redox pathways.[9] Here, we investigate the contribution of associative pathways at Pt/TiO_2 interface sites to the overall WGS reaction rate. Because computational studies[9,34,58,60] revealed that the active reaction intermediate in the associative mechanism is a carboxyl (-COOH) species rather than a formate (-HCOO) species and we have also shown that the formation and decomposition of a formate intermediate at Pt/CeO_2 interface sites requires overcoming high activation barriers compared to the carboxyl intermediate,[9] we focused in this study mainly on the associative carboxyl pathway at Pt/TiO_2 (110) interface sites.

The associative carboxyl pathway at the Pt/TiO_2 interface, as illustrated in Figure 1b, requires a five-coordinated Ti atom (Ti_{5c}) in the proximity of a Pt atom to adsorb and dissociate H_2O. Such a Ti_{5c} atom is in our model (Figure 2) available only next to corner Pt atoms. The reaction steps considered for this pathway at a corner Pt atom ($*_{Pt}$) are shown in eqs R1−R10:

$$*_{Pt}\ (IM1) + CO_{(g)} \rightarrow CO_{Pt}\ (IM2) \quad (R1)$$

$$CO_{Pt}\ (IM2) + *_{Ti} + H_2O_{(g)} \rightarrow CO_{Pt}{-}H_2O_{Ti}\ (IM3) \quad (R2)$$

$$CO_{Pt}{-}H_2O_{Ti}\ (IM3) + O_b \rightarrow CO_{Pt}{-}OH_{Ti}{-}O_bH\ (IM4) \quad (R3)$$

$$CO_{Pt}{-}OH_{Ti}{-}O_bH\ (IM4) \rightarrow COOH_{(Pt-Ti)}{-}O_bH\ (IM5) \quad (R4)$$

$$COOH_{(Pt-Ti)}{-}O_bH\ (IM5) + O_s \rightarrow CO_{2(Pt-Ti)}{-}O_bH{-}O_sH\ (IM6) \quad (R5)$$

$$CO_{2(Pt-Ti)}{-}O_bH{-}O_sH\ (IM6) \rightarrow *_{Pt}{-}O_bH{-}O_sH\ (IM7) + *_{Ti} + CO_{2(g)} \quad (R6)$$

$$*_{Pt}{-}O_bH{-}O_sH\ (IM7) + *_{Pt} \rightarrow *_{Pt}{-}H_{Pt}{-}O_bH\ (IM8) + O_s \quad (R7)$$

$$*_{Pt}{-}H_{Pt}{-}O_bH\ (IM8) + O_s \rightarrow *_{Pt}{-}H_{Pt}{-}O_sH\ (IM9) + O_b \quad (R8)$$

$$*_{Pt}{-}H_{Pt}{-}O_sH\ (IM9) \rightarrow 2H_{Pt}\ (IM10) + O_s \quad (R9)$$

dx.doi.org/10.1021/cs5009706 | ACS Catal. 2014, 4, 3654−3662

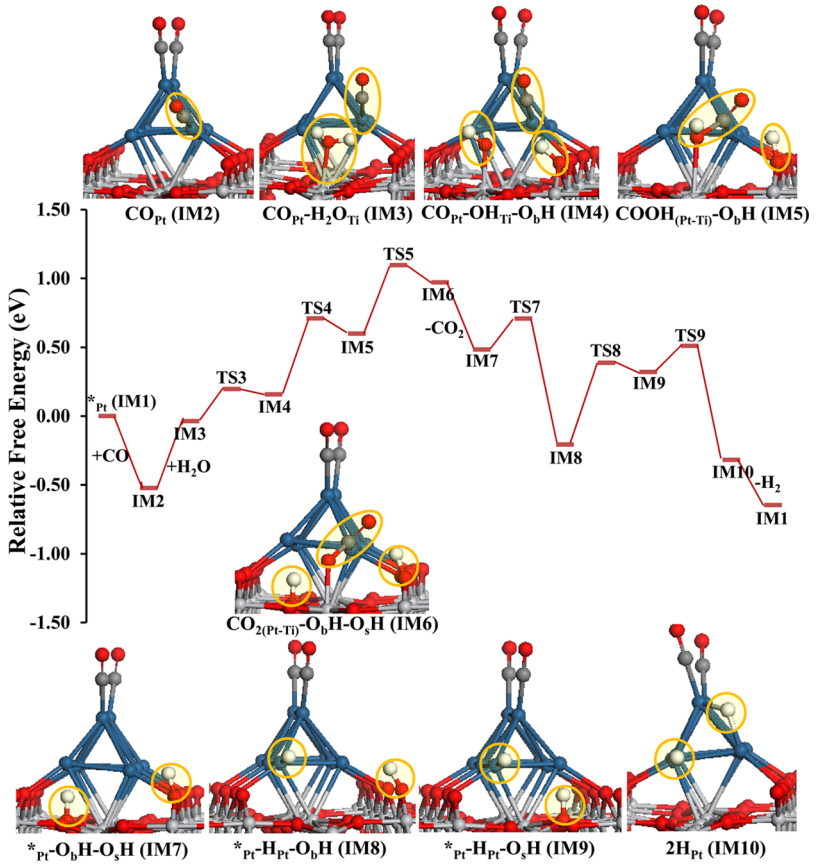

Figure 3. Free energy profile for the associative carboxyl pathway at a corner Pt atom of a Pt/TiO_2 (110) interface [T = 500 K; P_i(gas) = 1 atm]. All energies are with reference to the sum of the energies of the initial state (*$_{Pt}$, IM1) and the gas phase molecules.

$$2H_{Pt}\ (IM10) \rightarrow *_{Pt}\ (IM1) + H_{2(g)} + *_{Pt} \qquad (R10)$$

The calculated Gibbs free energy profile for this associative carboxyl pathway at a representative temperature of 500 K is illustrated in Figure 3. The partial pressures of the gas phase molecules were assumed to be 1 atm. The optimized intermediate structures are shown in the inset, and the TS structures are provided in the Supporting Information. We numbered the TS structures with reference to the elementary reaction steps throughout this paper. In the first elementary step, CO adsorbs on a corner interfacial Pt site with a binding free energy of −0.52 eV (reaction R1; ΔE_{ZPE} = −1.47 eV). H_2O adsorbs on a neighboring Ti_{5c} atom (reaction R2) and dissociates (reaction R3) by transferring a H atom to the bridging oxygen atom (O_b). Adsorption of H_2O on the oxide metal is endergonic (reaction R2; ΔE_{ZPE} = −0.41 eV), and the dissociation process (reaction R3) is also slightly endergonic by 0.19 eV with an activation free energy of 0.23 eV. We note here that the process of transferring the H atom from adsorbed H_2O (IM3) to either the Pt atom or a surface oxygen (O_s) requires activation barriers higher than that of reaction R3. In the following step (reaction R4), the CO adsorbed on a corner Pt site reacts with the -OH adsorbed on a Ti_{5c} site forming a -COOH intermediate (IM5). This process is again endergonic by 0.44 eV with a barrier of 0.55 eV. There are multiple possibilities for the dissociation of a -COOH species (reaction R5) because of the presence of different sites, such as O_s, O_b, O_bH, and Pt, adjacent to this species. The calculated transition states and reaction energies for the different possibilities of -COOH dissociation are provided in the Supporting Information. Our calculations suggested that -COOH dissociation is equally favorable on all these neighboring oxygen sites (activation barriers are within 0.1 eV); however, the barrier for transferring the H atom directly to the metal is higher than the corresponding barriers to oxygen sites. In agreement with earlier computational studies of the WGS reaction on Cu (111)[60] and Pt (111)[58] surfaces, as well as at Au/CeO_2 (111) interface sites,[34] our calculations predicted the lowest barrier for transferring the H from -COOH to the neighboring -O_bH, forming adsorbed CO_2 and -O_bHH species, respectively. Considering that the H atoms from the -O_bHH species have to be transferred to the Pt cluster through surface oxygen atoms (O_s) and the dissociation of -COOH to the neighboring O_s is equally favorable, we included the transfer of H from -COOH to Os (reaction R5) in our microkinetic model. The activation free energy of this dissociation process is 0.50 eV, and the process is endergonic by 0.47 eV. The corresponding TS (TS5, Figure 3) has the highest energy in the free energy profile.

The desorption of CO_2 from IM6 takes place in the next step (reaction R6; ΔG = −0.59 eV), leading to the formation of intermediate IM7 with two adsorbed H atoms on O_s and O_b. These H atoms are transferred to Pt in reaction steps R7−R9, forming a more stable intermediate IM10. The activation free energies of both H-transfer processes from O_s to Pt (reactions R7 and R9) are only ∼0.2 eV. Although transferring an H from O_b to O_s requires a barrier of 0.59 eV (reaction R8), the corresponding TS is lower than TS5 in the overall reaction free energy profile. The catalytic cycle is completed with the desorption of H_2 from IM10. Because the dissociative adsorption of H_2 on Pt (111) is barrierless,[58] we did not

dx.doi.org/10.1021/cs5009706 | ACS Catal. 2014, 4, 3654−3662

Table 1. Apparent Activation Energies (E_{app}) and Turnover Frequencies (TOF) for the Associative Carboxyl Pathway at the Corner Pt Atoms of the Pt/TiO_2 (110) Interface

reaction condition	method	TOF (s^{-1})	E_{app} (eV)	reaction order			
				CO	H_2O	CO_2	H_2
P_{CO} = 0.1 atm, P_{CO_2} = 0.1 atm, P_{H_2O} = 0.2 atm, P_{H_2} = 0.4 atm; T = 573 K	experiment[a]	6.0×10^{-1}	0.61	0.30	0.85	0.00	−0.67
	corner Pt[b]	1.5×10^{-3}	0.69	0.00	1.00	0.00	0.00
	edge Pt[c]	3.3×10	0.58	0.52	0.80	0.00	−0.16

[a]See ref 37. [b]From this work. [c]See ref 7.

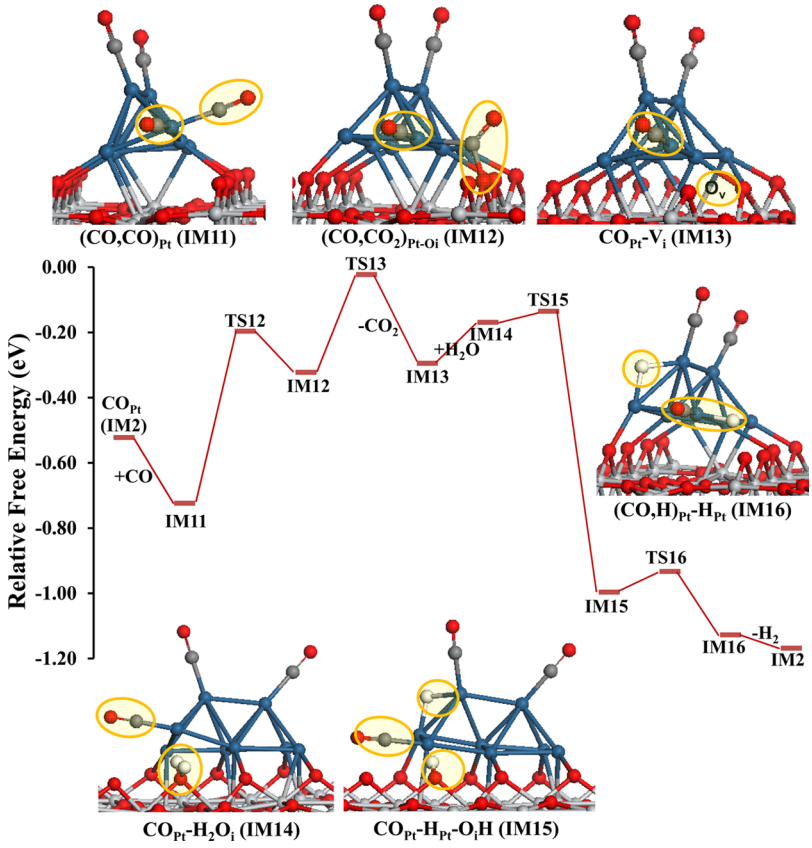

Figure 4. Free energy profile for the redox pathway at a corner Pt of a Pt/TiO_2 (110) interface [T = 500 K; P_i(gas) = 1 atm]. All energies are with reference to the sum of the energies of the initial state ($*_{Pt}$, IM1) and the gas phase molecules.

calculate the transition state for the desorption of H_2. In addition to the formation of a carboxyl intermediate [$COOH_{(Pt-Ti)}$−O_bH, IM5] in reaction R4, we also tested the possibility of forming a formate intermediate ($HCOO_{Ti}$−O_bH) from CO_{Pt}−OH_{Ti}−O_bH (IM4). Our calculations suggested that the formate intermediate is slightly more stable than the carboxyl intermediate by 0.2 eV. However, the formation of -HCOO species is highly unfavorable because of the required two-step process, H abstraction by CO forming a formyl intermediate (CHO_{Pt}−O_{Ti}−O_bH) and -CHO spillover from Pt to O_{Ti}. The formyl intermediate is less stable than IM4 by more than 1 eV, and its formation process requires surmounting an ∼1.5 eV barrier. Thus, we did not include these steps in our microkinetic model.

The kinetic parameters of the elementary steps calculated at different temperatures, i.e., ZPE-corrected reaction energies, activation barriers, forward rate constants, and equilibrium constants, are provided in the Supporting Information. As explained in Computational Model and Methods and also in our recent work,[7] we used these DFT data to build a microkinetic model of the WGS reaction. The experimental reaction conditions used in our microkinetic model are also similar to those used in our earlier work. The results obtained from our microkinetic model for the associative carboxyl pathway at a temperature of 573 K are provided in Table 1 together with the experimental results.[37] For comparison, we have also included our earlier results for the redox pathways at edge Pt sites[7] in this table. The microkinetic analysis of the associative carboxyl pathway predicts an apparent activation barrier of 0.69 eV, which is close to the experimental value of 0.61 eV. However, the calculated turnover frequency (TOF) is ∼2 orders of magnitude lower than the experimental value and 4 orders of magnitude lower than the redox pathway at edge Pt sites. Furthermore, computations predict a much higher reaction order with respect to H_2O and zero orders with respect to CO, CO_2, and H_2. As already suggested by the free energy profile, Campbell's degree of rate control analysis also points to -COOH dissociation as a rate-controlling process that is in agreement with an earlier report on the WGS over Pt (111).[58] Because of the strong adsorption of CO at the corner

dx.doi.org/10.1021/cs5009706 | ACS Catal. 2014, 4, 3654−3662

Table 2. Reaction Orders, Apparent Activation Energies (E_{app}), and Turnover Frequencies (TOF) Calculated from Our Microkinetic Model for the WGS Reaction at the Corner Pt Atoms of the Pt/TiO_2 (110) Interface under Different Experimental Reaction Conditions

reaction condition	method	TOF (s^{-1})[a]	E_{app} (eV)[b]	reaction order			
				CO	H_2O	CO_2	H_2
reaction condition 1; P_{CO} = 0.07 atm, P_{CO_2} = 0.09 atm, P_{H_2O} = 0.22 atm, P_{H_2} = 0.37 atm; T = 503 K	experiment[c]	0.13	0.58	0.30	0.68	0.00	−0.70
	corner Pt[d]	0.40	1.62	0.00	0.00	0.00	0.00
	edge Pt[e]	6.76	0.56	0.87	0.29	0.00	−0.90
reaction condition 2; P_{CO} = 0.03 atm, P_{CO_2} = 0.06 atm, P_{H_2O} = 0.1 atm, P_{H_2} = 0.2 atm; T = 523 K	experiment[f]	0.13	0.47	0.50	1.00	0.00	−0.70
	corner Pt[d]	0.40	1.57	0.01	0.01	0.00	0.00
	edge Pt[e]	4.23	0.46	0.79	0.53	0.00	−0.51
reaction condition 3; P_{CO} = 0.1 atm, P_{CO_2} = 0.1 atm, P_{H_2O} = 0.2 atm, P_{H_2} = 0.4 atm; T = 573 K	experiment[g]	0.60	0.61	0.30	0.85	0.00	−0.67
	corner Pt[d]	10.09	1.63	0.01	0.01	0.00	0.00
	edge Pt[e]	33.37	0.58	0.52	0.80	0.00	−0.16

[a]TOFs for reaction condition 1 were obtained at 523 K. [b]Apparent activation energies under all experimental conditions were calculated in the temperature range of 473−673 K. [c]See ref 23. [d]From this work. [e]See ref 7. [f]See ref 28. [g]See ref 37.

Pt site, the CO adsorbed structure (IM2) is the dominant intermediate in this associative carboxyl pathway throughout the temperature range considered here (interface coverage; $\theta_{IM2} \approx 1.0$). Campbell's degree of thermodynamic analysis further suggests that the stability of this intermediate strongly influences the rate of WGS. A similar observation was made in our recent work describing the redox and associative pathways of the WGS at Pt/CeO_2 (111) interface sites.[8,9] Further calculations in that case suggested that this strongly adsorbed CO could assist the WGS reaction at a neighboring site by reducing the CO adsorption strength. However, at the corner Pt atoms of the Pt/TiO_2 (110) interface, the CO adsorption energy at one corner Pt is not affected by the presence of CO at the neighboring Pt atom. Our calculations predict that the adsorption energy for CO at a neighboring corner Pt atom in the CO adsorbed intermediate (CO_{Pt}, IM2) is also as high as −1.5 eV. Thus, we do not expect that the co-adsorbed CO at corner Pt atoms will have any effect on the rates calculated for the associative carboxyl pathway.

3.2. Redox Pathway. Experimental studies of Pt/TiO_2 catalysts[22,25−27] mostly suggested that the redox pathway is dominant for the WGS reaction, and ^{18}O isotope experiments[28] provided strong evidence of the involvement of support oxygen in the process. Our computational study of the WGS reaction mechanism at an edge Pt atom of the Pt/TiO_2 (110) interface predicted high TOFs for the redox pathway.[7] Further analysis suggested that the reduced CO adsorption strength at the Pt/TiO_2 interface is one of the critical factors that contributes to the improved activity of these catalysts compared to Pt(111) or stepped Pt surfaces. Here, we investigate the redox pathway at a corner Pt where CO adsorption was found to be stronger than at the edge Pt. Because our analysis of the associative carboxyl pathway described in the previous section suggests that CO adsorbed on a corner Pt is stable over the temperature range of 473−673 K considered here, we chose this structure (CO_{Pt}, IM2) as the initial reactant model to investigate the redox pathway.

$$CO_{Pt}\ (IM2) + CO_{(g)} \rightarrow (CO, CO)_{Pt}\ (IM11) \quad (R11)$$

$$(CO, CO)_{Pt}\ (IM11) + O_i \rightarrow (CO, CO_2)_{Pt-O_i}\ (IM12) \quad (R12)$$

$$(CO, CO_2)_{Pt-O_i}\ (IM12) \rightarrow CO_{Pt}{-}V_i\ (IM13) + CO_{2(g)} \quad (R13)$$

$$CO_{Pt}{-}V_i\ (IM13) + H_2O_{(g)} \rightarrow CO_{Pt}{-}H_2O_i\ (IM14) \quad (R14)$$

$$CO_{Pt}{-}H_2O_i\ (IM14) + *_{Pt} \rightarrow CO_{Pt}{-}H_{Pt}{-}O_iH\ (IM15) \quad (R15)$$

$$CO_{Pt}{-}H_{Pt}{-}O_iH\ (IM15) \rightarrow (CO, H)_{Pt}{-}H_{Pt}\ (IM16) + O_i \quad (R16)$$

$$(CO, H)_{Pt}{-}H_{Pt}\ (IM16) \rightarrow CO_{Pt}\ (IM2) + H_{2(g)} + *_{Pt} \quad (R17)$$

The seven reaction steps considered for the redox pathway, starting from IM2, are described in eqs R11−R17, and the free energy profile calculated at 500 K is provided in Figure 4 together with the intermediate structures. The corresponding TS structures can be found in the Supporting Information. The first step in this pathway is CO adsorption on the corner Pt atom (reaction R11). Because the corner atoms are under-coordinated, the second CO adsorption on the same corner atom is still exergonic by −0.20 eV at 500 K. The adsorbed CO then spills over to the interface oxygen (reaction R12), creating an adsorbed CO_2 structure (IM12). The spillover is 0.40 eV endergonic and has an activation free energy of 0.52 eV (TS12). In the following step, CO_2 desorbs from the surface creating an oxygen vacancy at the interface (reaction R13). The desorption process is nearly energy neutral (ΔG = 0.03 eV) and requires an additional barrier of 0.30 eV (TS13). The reduced TiO_2 surface is then oxidized by the dissociation of H_2O at the vacancy. H_2O adsorbs on the oxygen vacancy (reaction R14; ΔE_{ZPE} = −0.77 eV) and easily dissociates by transferring one H atom to the Pt cluster (reaction R15), forming a stable intermediate, IM15. The second H from the interface oxygen is transferred to the metal in the following step (reaction R16), forming a slightly more stable intermediate, IM16 (ΔG = −0.13 eV). The activation free energies of both H-transfer processes are <0.1 eV. The last step is the desorption of H_2 from the Pt cluster (reaction R17; ΔG = −0.04 eV), which completes the catalytic cycle. The free energy profile (Figure 4) indicates that the TS corresponding to CO_2 desorption (TS13) is the highest-energy state in the reaction free energy profile. Because our earlier investigation[7] on the edge Pt atom revealed that the associative carboxyl/formate pathways with a redox regeneration route are less favorable than the redox pathway, we did not investigate those pathways at the corner Pt atom.

dx.doi.org/10.1021/cs5009706 | ACS Catal. 2014, 4, 3654−3662

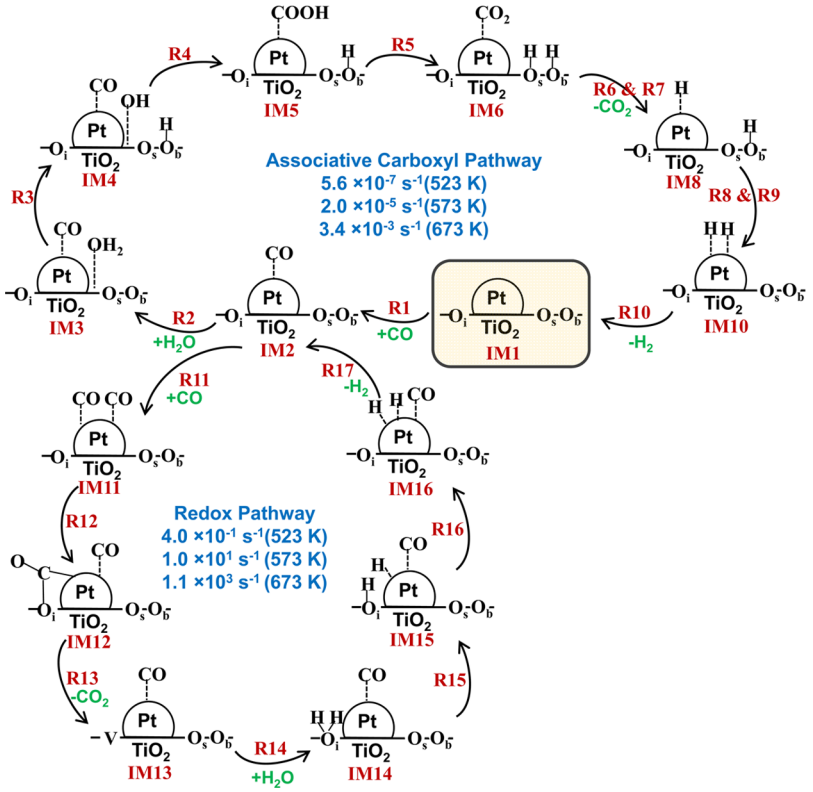

Figure 5. Network of possible WGS reaction steps at a corner Pt atom of a Pt_8/TiO_2 (110) interface.

3.3. Insights from Microkinetic Modeling. The free energy profiles calculated at 500 K for the associative carboxyl pathway (Figure 3) and the redox pathway (Figure 4) indicate that the redox pathway is energetically the most favorable pathway. To understand the effect of experimentally relevant temperatures and partial pressures of gas molecules on these pathways and also to obtain detailed information about the relative rates of these two pathways, reaction orders, and rate-determining steps, we built a DFT-based microkinetic model that includes all 17 elementary steps described above. The three experimental reaction conditions[23,28,37] used in our microkinetic model and the reported reaction orders, apparent activation energies (E_{app}), and turnover frequencies (TOFs) together with our calculated results are listed in Table 2. The kinetic parameters such as ZPE-corrected reaction energies, activation barriers, forward rate constants, and equilibrium constants for the 17 elementary steps are provided in the Supporting Information. The interface coverages of all intermediates calculated under different experimental conditions are also summarized in the Supporting Information.

A graphical representation of all elementary steps considered for the WGS reaction at the corner Pt of a Pt/TiO_2 interface is depicted in Figure 5. We have also provided in this figure the rates calculated at three different temperatures but under conditions (partial pressures) otherwise identical to reaction condition 3. The rates calculated for the associative carboxyl pathway at all three temperatures are ∼6 orders of magnitude smaller than rates for the redox pathway. The same trend is observed for experimental reaction conditions 1 and 2. Comparing these rates with the results presented in Table 1, we can see that the associative carboxyl pathway becomes even less favorable when we include the redox pathway in the microkinetic model as shown in Figure 5. Thus, the redox pathway is the dominant pathway at corner Pt atoms, and overall rates calculated for the corner Pt atoms in the temperature range of 523−573 K are close to those predicted for the edge Pt atoms (Table 2) in our recent report.[7] Below 523 K, the rates predicted by our model for the corner Pt atoms are ∼2 orders of magnitude lower than those of the edge Pt atoms, and above 573 K, the rates are ∼2 orders of magnitude higher than those of the edge Pt atoms. Consequently, the apparent activation barriers calculated for the corner Pt under all three reaction conditions are as high as 1.6 eV. These results suggest that the WGS reaction is highly favorable on the edge Pt atoms at low temperatures (473−573 K) and the corner Pt atoms become more active at higher temperatures (>573 K). Because the second CO adsorption at the corner Pt is also quite strong, the reaction order with respect to CO is predicted to be zero over the temperature range of 473−573 K. A slightly positive reaction order (0.25 at 673 K) was calculated at higher temperatures. Our model could not predict the experimentally observed positive and negative reaction orders with respect to H_2O and H_2, respectively, for the corner Pt atoms. However, these trends could be related to the WGS reaction occurring at the edge Pt atoms.

Campbell's degree of rate control analysis suggests that the CO_2 desorption process (reaction R13) is rate-controlling throughout the temperature range considered here. In our earlier investigation of the edge Pt atoms,[7] we also found that the CO_2 desorption process was rate-controlling in the classical redox pathway. Furthermore, adding a second CO molecule before CO_2 desorption also promoted this process and stabilized the oxygen vacancy structure. Hence, the second part of the redox pathway, H_2O dissociation and surface diffusion of H species, affected the overall rate more significantly. However, at the corner Pt atoms, CO_2 desorption

dx.doi.org/10.1021/cs5009706 | ACS Catal. 2014, 4, 3654−3662

Table 3. Campbell's Degree of Thermodynamic Rate Control (X_{TRC}) and Interface Coverages (θ) of Key Intermediates in the WGS Reaction at the Corner Pt Atoms of a Pt/TiO_2 (110) Interface

	reaction condition 1 (T = 503 K)		reaction condition 2 (T = 523 K)		reaction condition 3 (T = 573 K)	
intermediate	θ	X_{TRC}	θ	X_{TRC}	θ	X_{TRC}
CO_{Pt} (IM2)	7.49×10^{-4}	−0.04	4.75×10^{-3}	−0.10	1.30×10^{-2}	−0.13
$(CO,CO)_{Pt}$ (IM11)	9.99×10^{-1}	−0.96	9.94×10^{-1}	−0.90	9.86×10^{-1}	−0.87

is still rate-limiting even in the presence of a second CO molecule. This could be related to the stronger adsorption of CO on the corner Pt atom compared to the edge Pt atom (−1.22 eV vs −0.88 eV). In fact, our model predicts that the CO-adsorbed intermediate (IM11) is the dominant intermediate throughout the temperature range considered here. In Table 3, we summarized the interface coverages of the most dominant species and the results obtained from Campbell's degree of thermodynamic rate control (X_{TRC}) analysis. The interface coverages of all species calculated under the three reaction conditions are provided in the Supporting Information. Campbell's degree of thermodynamic analysis also suggests that the stability of intermediate IM11 has a significant effect on the overall rate of reaction. Above 573 K, this species becomes less stable, which in turn dramatically increases the rate.

As a cautionary note, we mention that the trends in rates predicted by our model are directly related to the CO adsorption strengths at different sites. It has been suggested that the PBE functional used in our calculations underestimates the gas phase energy of the CO molecule, which in turn overestimates the gas phase reaction enthalpy of the water−gas shift reaction.[61] For our current computational setup, the overall error in the water−gas shift reaction free energy is calculated to be 0.43 eV. In agreement with the earlier report by Peterson et al.,[61] a statistical analysis of a set of gas phase reactions, including species CO, H_2O, CO_2, and H_2, suggested that the error lies mostly on the CO molecule. Adding this correction to the gas phase energy of CO molecule in our microkinetic model of the WGS reaction on the corner Pt atoms decreases the rates at higher temperatures and subsequently reduces the apparent activation barrier to 0.64 eV. The redox pathway at the corner Pt atom is still the dominant pathway compared to the associative carboxyl pathway. However, it is currently unknown how much of this error in the gas phase energy of the CO molecule is transferred to the CO-adsorbed intermediates and transition states. This error propagation can be understood only by considering uncertainties in all elementary rate and equilibrium constants through statistical (Bayesian) error analysis.[62] We plan to quantify the uncertainty in calculated rates using this approach in a future study.

4. CONCLUSIONS

We investigated the redox and associative carboxyl pathways of the WGS reaction at a corner Pt atom of a Pt/TiO_2 (110) interface model. Our microkinetic analysis based on parameters obtained from first principles (without any fitting parameters) predicts that the WGS reaction follows the redox pathway at the Pt/TiO_2 (110) interface. The rates calculated for the associative carboxyl pathway are ∼6 orders of magnitude smaller than those of the redox pathway, suggesting that the oxygen vacancy structure plays an essential role in promoting H_2O adsorption and dissociation. In the associative carboxyl pathway, H_2O dissociation on the Ti metal site is endothermic as in the case of the Pt (111) surface. Although the activation barriers for individual elementary reactions in the associative carboxyl pathway are less than 0.6 eV, the stability of adsorbed species -OH, -COOH, and -CO_2 continuously decreases along the catalytic cycle, which in turn increases the apparent activation barrier and decreases the rate. On the other hand, H_2O dissociation is highly exothermic at an oxygen vacancy site, promoting the redox pathway. Comparing the rates calculated for the redox pathways at the corner Pt atom with those of our previously investigated edge Pt atom, we find that the calculated rates for the corner Pt atoms are ∼2 orders of magnitude lower below 523 K and 2 orders of magnitude higher above 573 K than those of the edge Pt atoms. In contrast to the results obtained for the edge Pt atoms, CO_2 desorption is rate-limiting at the corner Pt atoms because of strong adsorption of CO. Thus, the rates at the corner Pt atoms increase dramatically above 573 K, when the adsorption becomes thermodynamically less favorable. On the basis of these results, we suggest that the edge Pt atoms at the Pt/TiO_2 (110) interface are active for the WGS reaction at low temperatures and the corner Pt atoms contribute more to the overall rate at higher temperatures. Overall, our findings confirm that the redox pathway is the dominant pathway for the WGS reaction at Pt/TiO_2 (110) interface sites and oxygen vacancies on the TiO_2 surface play a critical role in WGS activity.

■ ASSOCIATED CONTENT

Supporting Information

Reaction energies, activation barriers, and kinetic parameters for the elementary steps considered in the redox and associative carboxyl pathways; calculated transition state structures for the associative carboxyl and redox pathways; and different possibilities for the dissociation of the carboxyl intermediate. This material is available free of charge via the Internet at http://pubs.acs.org.

■ AUTHOR INFORMATION

Corresponding Author

*E-mail: heyden@cec.sc.edu.

Notes

The authors declare no competing financial interest.

■ ACKNOWLEDGMENTS

This work was supported by National Science Foundation Grant CBET-0932991 and in part by Grant CBET-1254352 and XSEDE resources provided by the National Institute for Computational Sciences (NICS) and the Texas Advanced Computing Center (TACC) under Grant TG-CTS090100. Furthermore, a portion of this research was performed at the U.S. Department of Energy facilities located at the National Energy Research Scientific Computing Center (NERSC) and at EMSL, located at Pacific Northwest National Laboratory (Grant Proposal 47447). Finally, computing resources from

the University of South Carolina's High Performance Computing Group are gratefully acknowledged.

REFERENCES

(1) Haller, G. L.; Resasco, D. E. *Adv. Catal.* **1989**, *36*, 173−235.
(2) Schwab, G. M. *Angew. Chem., Int. Ed.* **1967**, *6*, 375.
(3) Hayek, K.; Kramer, R.; Paal, Z. *Appl. Catal., A* **1997**, *162*, 1−15.
(4) Libuda, J.; Freund, H. J. *Surf. Sci. Rep.* **2005**, *57*, 157−298.
(5) Green, I. X.; Tang, W. J.; Neurock, M.; Yates, J. T. *Science* **2011**, *333*, 736−739.
(6) Wu, Y. Y.; Mashayekhi, N. A.; Kung, H. H. *Catal. Sci. Technol.* **2013**, *3*, 2881−2891.
(7) Ammal, S. C.; Heyden, A. *J. Catal.* **2013**, *306*, 78−90.
(8) Aranifard, S.; Ammal, S. C.; Heyden, A. *J. Catal.* **2014**, *309*, 314−324.
(9) Aranifard, S.; Ammal, S. C.; Heyden, A. *J. Phys. Chem. C* **2014**, *118*, 6314−6323.
(10) Hinrinchsen, K.-O.; Kochloefl, K.; Muhler, M. *Handbook of Heterogeneous Catalysis*; Wiley-VCH: Weinheim, Germany, 2008.
(11) Burch, R. *Phys. Chem. Chem. Phys.* **2006**, *8*, 5483−5500.
(12) Liu, P.; Rodriguez, J. A. *J. Chem. Phys.* **2007**, *126*, 164705.
(13) Zalc, J. M.; Sokolovskii, V.; Loffler, D. G. *J. Catal.* **2002**, *206*, 169−171.
(14) Azzam, K. G.; Babich, I. V.; Seshan, K.; Lefferts, L. *J. Catal.* **2007**, *251*, 163−171.
(15) Bunluesin, T.; Gorte, R. J.; Graham, G. W. *Appl. Catal., B* **1998**, *15*, 107−114.
(16) Wang, J.; Kispersky, V. F.; Delgass, W. N.; Ribeiro, F. H. *J. Catal.* **2012**, *289*, 171−178.
(17) Shekhar, M.; Wang, J.; Lee, W. S.; Williams, W. D.; Kim, S. M.; Stach, E. A.; Miller, J. T.; Delgass, W. N.; Ribeiro, F. H. *J. Am. Chem. Soc.* **2012**, *134*, 4700−4708.
(18) Fu, Q.; Saltsburg, H.; Flytzani-Stephanopoulos, M. *Science* **2003**, *301*, 935−938.
(19) Fu, Q.; Deng, W. L.; Saltsburg, H.; Flytzani-Stephanopoulos, M. *Appl. Catal., B* **2005**, *56*, 57−68.
(20) Rodriguez, J. A.; Ma, S.; Liu, P.; Hrbek, J.; Evans, J.; Perez, M. *Science* **2007**, *318*, 1757−1760.
(21) Mudiyanselage, K.; Senanayake, S. D.; Feria, L.; Kundu, S.; Baber, A. E.; Graciani, J.; Vidal, A. B.; Agnoli, S.; Evans, J.; Chang, R.; Axnanda, S.; Liu, Z.; Sanz, J. F.; Liu, P.; Rodriguez, J. A.; Stacchiola, D. J. *Angew. Chem., Int. Ed.* **2013**, *52*, 5101−5105.
(22) Williams, W. D.; Shekhar, M.; Lee, W. S.; Kispersky, V.; Delgass, W. N.; Ribeiro, F. H.; Kim, S. M.; Stach, E. A.; Miller, J. T.; Allard, L. F. *J. Am. Chem. Soc.* **2010**, *132*, 14018−14020.
(23) Pazmino, J. H.; Shekhar, M.; Williams, W. D.; Akatay, M. C.; Miller, J. T.; Delgass, W. N.; Ribeiro, F. H. *J. Catal.* **2012**, *286*, 279−286.
(24) Shekhar, M.; Wang, J.; Lee, W. S.; Akatay, M. C.; Stach, E. A.; Delgass, W. N.; Ribeiro, F. H. *J. Catal.* **2012**, *293*, 94−102.
(25) Azzam, K. G.; Babich, I. V.; Seshan, K.; Lefferts, L. *J. Catal.* **2007**, *251*, 153−162.
(26) Vignatti, C.; Avila, M. S.; Apesteguia, C. R.; Garetto, T. F. *Int. J. Hydrogen Energy* **2010**, *35*, 7302−7312.
(27) Panagiotopoulou, P.; Kondarides, D. I. *Catal. Today* **2006**, *112*, 49−52.
(28) Kalamaras, C. M.; Panagiotopoulou, P.; Kondarides, D. I.; Efstathiou, A. M. *J. Catal.* **2009**, *264*, 117−129.
(29) Rodriguez, J. A.; Evans, J.; Graciani, J.; Park, J. B.; Liu, P.; Hrbek, J.; Sanz, J. F. *J. Phys. Chem. C* **2009**, *113*, 7364−7370.
(30) Liu, Z. P.; Jenkins, S. J.; King, D. A. *Phys. Rev. Lett.* **2005**, *94*, 196102.
(31) Iida, H.; Igarashi, A. *Appl. Catal., A* **2006**, *298*, 152−160.
(32) Panagiotopoulou, P.; Christodoulakis, A.; Kondarides, D. I.; Boghosian, S. *J. Catal.* **2006**, *240*, 114−125.
(33) Kalamaras, C. M.; Gonzalez, I. D.; Navarro, R. M.; Fierro, J. L. G.; Efstathiou, A. M. *J. Phys. Chem. C* **2011**, *115*, 11595−11610.
(34) Chen, Y.; Wang, H. F.; Burch, R.; Hardacre, C.; Hu, P. *Faraday Discuss.* **2011**, *152*, 121−133.
(35) Ammal, S. C.; Heyden, A. *J. Phys. Chem. C* **2011**, *115*, 19246−19259.
(36) Pozdnyakova, O.; Teschner, D.; Wootsch, A.; Krohnert, J.; Steinhauer, B.; Sauer, H.; Toth, L.; Jentoft, F. C.; Knop-Gericke, A.; Paal, Z.; Schlogl, R. *J. Catal.* **2006**, *237*, 1−16.
(37) Thinon, O.; Rachedi, K.; Diehl, F.; Avenier, P.; Schuurman, Y. *Top. Catal.* **2009**, *52*, 1940−1945.
(38) Kresse, G.; Furthmuller, J. *Phys. Rev. B* **1996**, *54*, 11169−11186.
(39) Kresse, G.; Furthmuller, J. *Comput. Mater. Sci.* **1996**, *6*, 15−50.
(40) Kresse, G.; Hafner, J. *Phys. Rev. B* **1993**, *47*, 558−561.
(41) Kresse, G.; Hafner, J. *Phys. Rev. B* **1994**, *49*, 14251−14269.
(42) Perdew, J. P.; Burke, K.; Ernzerhof, M. *Phys. Rev. Lett.* **1996**, *77*, 3865−3868.
(43) Blochl, P. E. *Phys. Rev. B* **1994**, *50*, 17953−17979.
(44) Kresse, G.; Joubert, D. *Phys. Rev. B* **1999**, *59*, 1758−1775.
(45) Makov, G.; Payne, M. C. *Phys. Rev. B* **1995**, *51*, 4014−4022.
(46) Harris, J. *Phys. Rev. B* **1985**, *31*, 1770−1779.
(47) Henkelman, G.; Uberuaga, B. P.; Jónsson, H. *J. Chem. Phys.* **2000**, *113*, 9901−9904.
(48) Heyden, A.; Bell, A. T.; Keil, F. J. *J. Chem. Phys.* **2005**, *123*, 224101.
(49) Olsen, R. A.; Kroes, G. J.; Henkelman, G.; Arnaldsson, A.; Jonsson, H. *J. Chem. Phys.* **2004**, *121*, 9776−9792.
(50) Stegelmann, C.; Andreasen, A.; Campbell, C. T. *J. Am. Chem. Soc.* **2009**, *131*, 8077−8082.
(51) Newsome, D. S. *Catal. Rev.* **1980**, *21*, 275−318.
(52) Shido, T.; Iwasawa, Y. *J. Catal.* **1992**, *136*, 493−503.
(53) Shido, T.; Iwasawa, Y. *J. Catal.* **1993**, *141*, 71−81.
(54) Jacobs, G.; Khalid, S.; Patterson, P. M.; Sparks, D. E.; Davis, B. H. *Appl. Catal., A* **2004**, *268*, 255−266.
(55) Jacobs, G.; Williams, L.; Graham, U.; Sparks, D.; Davis, B. H. *J. Phys. Chem. B* **2003**, *107*, 10398−10404.
(56) Meunier, F. C.; Tibiletti, D.; Goguet, A.; Shekhtman, S.; Hardacre, C.; Burch, R. *Catal. Today* **2007**, *126*, 143−147.
(57) Stamatakis, M.; Chen, Y.; Vlachos, D. G. *J. Phys. Chem. C* **2011**, *115*, 24750−24762.
(58) Grabow, L. C.; Gokhale, A. A.; Evans, S. T.; Dumesic, J. A.; Mavrikakis, M. *J. Phys. Chem. C* **2008**, *112*, 4608−4617.
(59) Burch, R.; Goguet, A.; Meunier, F. C. *Appl. Catal., A* **2011**, *409*, 3 and references cited therein.
(60) Gokhale, A. A.; Dumesic, J. A.; Mavrikakis, M. *J. Am. Chem. Soc.* **2008**, *130*, 1402−1414.
(61) Peterson, A. A.; Abild-Pedersen, F.; Studt, F.; Rossmeisl, J.; Norskov, J. K. *Energy Environ. Sci.* **2010**, *3*, 1311−1315.
(62) Ulissi, Z.; Prasad, V.; Vlachos, D. G. *J. Catal.* **2011**, *281*, 339−344.